Design and Kinematic Analysis of a Multi-Grip Hand– Touch Hand 4

Kiran Setty and Theo Van Niekerk
Nelson Mandela University, Port Elizabeth, South Africa
Email: kiransettyks@gmail.com, theovanniekerk@mandela.ac.za

Riaan Stopforth and Karina Sewsunker
Stopforth Mechatronics, Robotics and Research Lab, University of KwaZulu-Natal, Durban, South Africa
Email: stopforth.research@gmail.com, karinsewsunker@gmail.com

Anton du Plessis
Stellenbosch University, Stellenbosch, South Africa
Email: anton2@sun.ac.za

***Abstract*—This paper reports on the kinematic design of the Touch Hand 4, which has been a continuous optimization of the first three iterations. The Touch Hand 4 is a low-cost myoelectric prosthetic terminal hand device designed to be used by transradial amputees. The paper investigates the mechanical design of the prosthetic hand and investigates the kinematics and static force analysis of the digits on the hands. Illustrative diagrams describe the kinematics and static force analysis. The analysis results are displayed and used to compare the different digits designed on the prosthetic hand. The final product is then tested and compared with other prosthetic hands. The Touch Hand 4 had shown in tests to perform significantly slower than other prosthetic hands but had similar grip strength to some prosthetic hands.**

***Index Terms*—prosthetic hand, multi-grip, 3D printed, touch hand**

I. Introduction

The Bebionic is considered the most cost-effective myoelectric prosthetic hand on the market, costing between $25000 to $35000 [1]. This prosthetic hand controls each digit with an individual motor, thus allowing for various grips. However, this prosthetic hand has a significantly weaker grip force than the other more expensive prosthetic devices. [2]

The i-Limb Ultra is considered to have the most lifelike natural movement of the hand, having a price of $120 000 for the model containing all the essential features [3]. Whist also using individual motors for each digit, this hand can perform various grips. These grips, however, are controlled by a mobile app. The i-Limb can perform 14 different hand gestures; however, it comes with an optional power thumb, which allows the user to perform an additional four hand gestures and increase the grip strength. This optional addition is the primary cause of the range in the price. [4]

The Michelangelo is considered the most aesthetically pleasing with the most human-like appearance, costing $73 800 [5]. Of all the mechanical designs of the three prosthetic hands being discussed, the Michelangelo is the most unique as it uses only one motor to close all five digits [6]. The use of only one motor allows for this hand to be the lightest of all the hands relative to their size. Given that all the digits open and close together, there are significantly fewer hand gestures that can be performed with this hand than the others. Given the strength of the hand's lateral grip, Ottobock states that amputees are more likely to use this grip every day, allowing them to grab objects more easily. [7]

A 3D printed prosthetic hand, named X-Limb, was designed to weigh 253 grams, with a grip force of 21.5N [8]. The cost of this hand is 200 USD, excluding costs of a disconnecting wrist [8]. Furthermore, the minimum lifetime of this device is one year.

The deficiencies in current prosthetic hand devices are the lack of grip switching and grip interlocking [9]. Therefore, a study was performed to develop a low-cost myoelectric prosthetic terminal hand device for transradial amputees. The prosthetic device is low-cost while also providing the function of a commercially available prosthetic hand. The mechanical design of the prosthetic hand incorporates modularity of the components to allow for the easy service, repair, and replacement of parts. The research of the Touch Hand 4 is a continuation of the Touch Hand 2 [10] and the Touch Hand 3 [11]. The research showed how a prosthetic hand with a manufacturing cost of only $967.84 could be made cheap using cheaper components, materials, and manufacturing methods while being functional by optimizing the kinematics of the device to enhance the grip.

This paper has the following research contributions:

Manuscript received February 4, 2022; revised June 8, 2022.
Corresponding author: Riaan Stopforth.

doi: 10.18178/ijmerr.11.7.466-478

- The research investigated various digit designs by analyzing the design relative to prehensile grip patterns.
- The kinematics and statics of the digits were analyzed with the kinematic analysis and static force analysis programs, showing the capability of the kinematics and static force analysis programs.
- The design of a mechanical system of a prosthetic hand capable of gripping objects of various sizes utilizing the fewest degrees of freedom in motion.

II. Mechanical Design of Touch Hand 4

The mechanical design process began with performing a literature review on research material and studies that discussed the kinematics of the human hand and how the degrees of freedom (DoF) of the hand are utilized to grip various objects [12]. The biokinematics of the human hand were also evaluated to emulate aspects of the design of the human hand in the Touch Hand 4 [13]. The DoF of the human hand was reviewed to determine what motions of the hand are most essential for gripping objects [14], [15]. Since the human hand has 26 DoF, it was not feasible to design a biomimetic prosthetic hand as each DoF would be required to be actuated by a motor [16]. Therefore, the DoF was reviewed by evaluating the motion of the hand as a whole when gripping objects and the most crucial DoF used in gripping objects.

The Touch Hand 4 is a terminal device; therefore, the device's design has a greater focus on the functions it performs rather than being visually and kinematically similar to the human hand [17]. Therefore, the prehensile capabilities of a hand are fundamental for its operation and are therefore essential to research to investigate the required operations from a prosthetic hand device. Prehension with the human hand is a dynamic matter with subtle variances, depending on the object manipulated, the object's physical properties, and the intention to use/manipulate the object [18]. Classification of prehension is attempted by categorizing the most used prehensions.

The six grips were evaluated according to the type of objects they are used to carry and their specific function. These grips include cylindrical grasp, tip, hook or snap, palmar, spherical grasp, and lateral [18].

Feedback received from the Touch Hand 2 [10] , and the Touch Hand 3 [19] was reviewed to help decide the suitable features to include in Touch Hand 4. Furthermore, from the interviews with prosthetists who work with many amputees from low-income households [20] [21] [22] [17] and with professionals who work on miscellaneous other prosthetic devices [23], the following are the design features, which were chosen to be implemented for the Touch Hand 4:

- The design shall have only three digits. It was assumed that the control system would not be capable of obtaining the accuracy to implement individual control of 5 digits; therefore, reducing the number of digits to 3 would not significantly affect the operation of the device.
- Each digit should be placed on the palm at a different angle, similar to the human hand, to allow the device to grip spherical objects.
- The thumb should move from the Carpometacarpal (CMC) joint rather than from the Metacarpophalangeal (MCP) joint to allow the thumb to move similar to a human hand. This would allow the device to reshape the palm when gripping the object and allow for a more natural grip.
- The digit flexion of the digits should be designed so that when the digits have achieved full flexion, the digits' tips meet at a singular point to allow the device to pick up small objects.

A picture of the CAD model of the Touch Hand 4 and the 3D, printed, fully assembled version can be seen in Fig. 1.

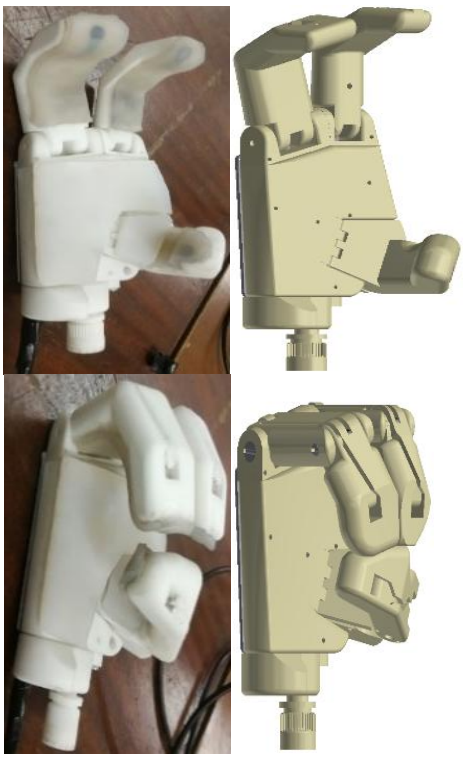

Figure 1. CAD model of Touch Hand 4 with static digits

III. Mechanical and Actuator Integration

The linear actuator used to actuate the digits is the Firgelli PQ12. The Firgelli linear actuator was chosen for the following reasons: [24]

- The linear actuator has a length of 41.5 mm when the shaft is fully retracted.
- The stroke length of the linear actuator is 20 mm, which is sufficient for all the digits designed.
- The linear actuator can apply a maximum of 50 N.

Flexion and adduction of the digits cause a cavity in the palm to form, forming topographical arches that assist the hand's grip in various manners. The arches of the hand are features that are used to simplify the mechanics of the reshaping of the hand. The hand arches have been discussed to determine how they affect the grip of the

human hand and how they could be implemented in the design of the Touch Hand 4.

The distal transverse arch was considered to be implemented in the Touch Hand 4 but would require reshaping the palm of the Touch Hand 4 itself. It was considered to implement the arches by means of soft padding in the palm, ensuring reshaping of the pad according to objects being grabbed. The longitudinal arch would be implemented by flexion and extension of the digits of the Touch Hand 4; however, it would only extend from the tips of the digits to the MCP joint since the palm is static. The oblique arch would be implemented with the flexion of the thumb and digit at the other end of the hand.

Research was performed on reducing the number of variables used to perform cylindrical and spherical grips on objects using principal component analysis (PCA). PCA reduces the motions of the hand to 5 variables with minimal deviation from the original shape. The PCA of the human hand was used to further reduce the least required DoF of the human hand to ensure the actuation of the hand using only the most important movements. The following are the considerations of the five simplified movements of the principal component analysis:

- The flexion/extension of the digits' MCP joints are considered essential to gripping objects and would therefore be implemented.
- The flexion/extension of the Proximal interphalangeal (PIP) and Distal interphalangeal (DIP) joints of the digits are considered to play an essential role in adapting to the shapes of objects and would therefore be implemented.
- The flexion/extension of the CMC joints of the ring finger and little finger shall be compromised by placing the digits at an angle rather than parallel to the index and ring finger.
- The adduction/abduction of all the digits was not considered as this was not feasible to be implemented effectively.
- The adduction/abduction of the MCP joint of the thumb was not considered as this motion was not effectively controlled even if the mechanical design incorporated this movement in the kinematics.

Since the principal component analysis was conducted only on human hands performing the cylindrical and spherical grip, the research was considered only to enhance the cylindrical and spherical grip and not any other grip. The results from the PCA were assumed to be useful to be considered in the conceptual design but may need changing to accommodate for other grips.

The base of the hand consists of the palm and the wrist, which connects to the socket of the amputee and to which the digits connect. The palm of the hand houses the linear actuators for the index and ring fingers, the geared DC motor for the wrist, and the wiring for the motors and force sensors. The palm is covered by a stainless-steel plate, which acts as a chassis. This is used to screw the motors and digits into place. It acts as a cover to protect the motors and wires. The wrist uses a motor to drive spur gears, rotating the wrist. Wires from the motors and sensors run from the palm to the wrist, where they run to the control boards, which power and control the motors. The connection of the wrist, which connects to the socket, is of industry standard and can be replaced to suit sockets designed to connect to different fittings.

Actuation of the interphalangeal joints in the index and ring finger differs from the actuation method used for the base joint in the design of the Touch Hand 4 since the decision has been made to not actuate the intermediate and distal phalanges with its own motor. It was considered to under-actuate the digits.

The static digit involves not moving the intermediate and distal phalange relative to the proximal phalange and having the entire digit moving as one.

The base joint of the index and ring finger is the MCP joint and the base joint of the thumb. The linking mechanisms for these designs are intended to connect the proximal phalange of the digits to their own respective motor to use the motion of the motor to turn the digit. Mechanisms that use gears were not considered since it was considered that the tolerance of Selective Laser Sintering (SLS) was not sufficient to ensure gears small enough to fit in the digits could be implemented without slippage.

The direct external connection involves connecting the end of the linear actuator's shaft to the proximal phalange with a revolute joint. The base of the linear actuator was designed to secure the palm with a revolute joint. Extension of the shaft causes flexion of the phalange. Rotation of the phalange causes the linear actuator to rotate about the revolute joint on the palm.

IV. Kinematics and Static Force Analysis

For the kinematics of the design to operate as required, correct dimensioning of the linkage systems needs to be implemented. Therefore, a program was written to calculate dimensions and simulate the kinematics of the linking mechanisms being designed. A program was also written to perform a static force analysis on the links involved in the linking mechanisms to determine the maximum stress experienced by each link and the maximum theoretical force the digits can apply on an object being gripped.

All the variables involved should be mathematically defined before the program development for the linking mechanisms. These calculations were performed using 2D diagrams of the linking mechanisms and trigonometry to calculate the variables relative to one another. Kinematic analyses have not been conducted on the asynchronous digits since they contained two DoF and therefore could not be defined. In designing the synchronous digits, the kinematic analysis helped measure the initial and final joint angles as a function of the designer's basic movement requirements. The design was evaluated based on static force analysis to determine the feasibility of the design.

A. Static Thumb Calculations

The linking mechanism for the static thumb consists of a three-bar mechanism with one of the bars changing in length, thus changing the angles of the bars in the system. This mechanism is present in the synchronous thumb;

however, the synchronous thumb also contains a synchronous mechanism to rotate the PIP joint. Fig. 2(a) shows the thumb super-imposed onto a cross-sectional view of the design. The linking mechanism displayed in Fig. 2(a) has been displayed more clearly in Fig. 2(b) to perform the calculations.:

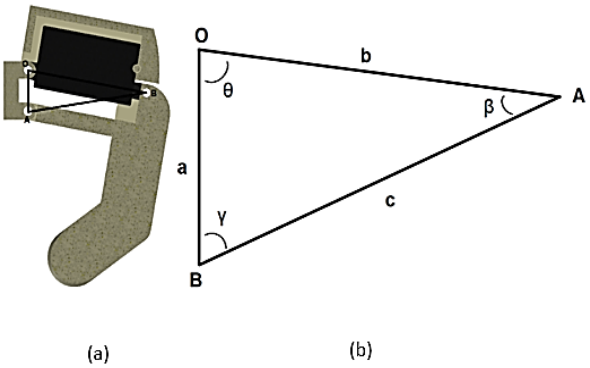

Figure 2. Diagram of static thumb super-imposed on the cross-section of CAD model

The links shown in Fig. 2(b) represent the following parts:

a – Base joint
b – Motor
c –Phalanges
θ – Base joint angle relative to the motor
β – Motor angle relative to phalanges
μ - Phalanges angle relative to base joint

The calculations performed to determine the angles of all the links require using the cosine rule and the sine rule. The following equation is the cosine rule [25]:

$$a^2 = b^2 + c^2 - 2 \cdot c \cdot b \cdot \cos(A) \tag{1}$$

where:

a – The first side of a triangle
b – The second side of a triangle
c – The third side of a triangle
A – The angle opposite the first side of a triangle

Eq. 2 is the sine rule [25]:

$$\frac{a}{\sin(A)} = \frac{b}{\sin(B)} = \frac{c}{\sin(C)} \tag{2}$$

where:

a – The first side of a triangle
b – The second side of a triangle
c – The third side of a triangle
A – The angle opposite the first side of a triangle
B – The angle opposite the second side of a triangle
C – The angle opposite the third side of a triangle

The first calculation uses the cosine rule in the triangle OAB:

$$c^2 = a^2 + b^2 - 2 \cdot a \cdot b \cdot \cos(\theta) \tag{3}$$

From equation 3, equation 4 is obtained for calculating θ:

$$\theta = \arccos\left(\frac{b^2 + a^2 - c^2}{2 \cdot b \cdot a}\right) \tag{4}$$

Equation 5 uses the sine rule in the triangle OAB:

$$\frac{c}{\sin(\theta)} = \frac{a}{\sin(\beta)} \tag{5}$$

From equation 5, equation 6 is obtained for calculating β:

$$\beta = \arcsin\left(\frac{a \cdot \sin(\theta)}{\sin(\beta)}\right) \tag{6}$$

B. Synchronous Digit Calculation

The synchronous digit acts as a four-bar linkage system to utilize rotation from the MCP joint to rotate the PIP phalange. The linking mechanism in the index and ring fingers differs from the mechanism in the thumb. Therefore, different diagrams are shown to represent each mechanism. The calculations, however, are performed in the same manner. The linking mechanism for the synchronous index and ring finger can be seen in Fig. 3(b). Furthermore, Fig. 3(a) shows the diagram super-imposed onto a cross-sectional view of the designed synchronous ring finger.

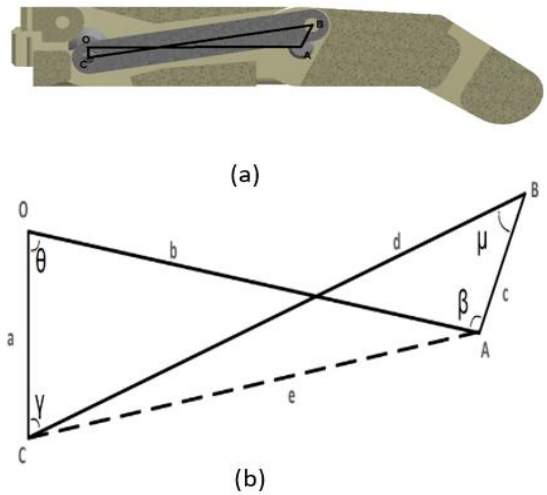

Figure 3. Diagram of the synchronous index and ring finger

The links shown in Fig. 3(b) represent the following parts:

a – MCP joint
b – Proximal phalange
c – Distal phalange
d – Connecting link between the MCP joint and the proximal phalange
e – Imaginary line drawn to perform calculations
θ – Proximal phalange angle relative to MCP joint
β – Distal phalange angle relative to proximal phalange
μ - Connecting link angle relative to distal phalange

γ – Connecting link angle relative to MCP joint

The linking mechanism in the thumb is responsible for synchronous movement. Unlike the mechanism for the index and ring finger, the thumb does not consist of the entire linking mechanism of the digit. Since the rotation of the MCP link requires a linking mechanism, the linking mechanism for synchronous movement is an addition to the linking mechanism present in the static thumb. The linking mechanism for the synchronous mechanism of the synchronous thumb can be seen in Fig. 4(a). Fig. 4(b) shows the diagram super-imposed onto a cross-sectional view of the designed synchronous thumb:

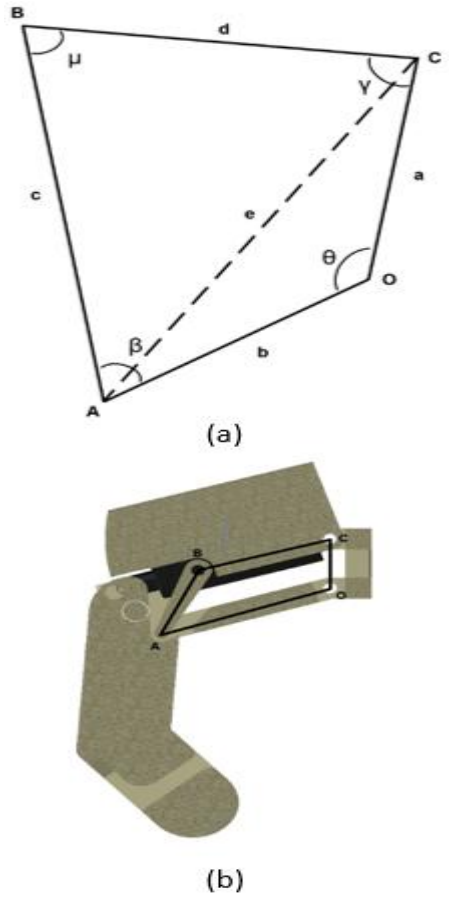

Figure 4. Diagram of the joint coupling mechanism of thumb

The links shown in Fig. 4(a) represent the following parts:

a – MCP joint

b –Phalanges

c – Connecting link between the MCP joint and the proximal phalange

d – Top link

e – Imaginary line drawn to perform calculations

θ – Bottom link angle relative to MCP joint

β – Connecting link angle relative to phalanges

μ - Connecting link angle relative to top link

γ – Top link angle relative to MCP joint

Equation 7 uses the cosine rule in the triangle OAC:

$$e^2 = a^2 + b^2 - 2 \cdot a \cdot b \cdot \cos(\theta) \quad (7)$$

Equation 8 uses the cosine rule for the triangle ABC:

$$e^2 = c^2 + d^2 - 2 \cdot c \cdot d \cdot \cos(\mu) \quad (8)$$

Equation 7 and Equation 8 are then combined to obtain equation 9:

$$c^2 + d^2 - 2 \cdot c \cdot d \cdot \cos(\mu) = a^2 + b^2 - 2 \cdot a \cdot b \cdot \cos(\theta) \quad (9)$$

From equation 9, equation 10 is obtained for calculating μ:

$$\mu = \arccos\left(\frac{c^2+d^2-a^2-b^2+2\cdot a\cdot b\cdot\cos(\theta)}{2\cdot c\cdot d}\right) \quad (10)$$

Using equation 7, equation 11 is obtained for calculating e:

$$e = \sqrt{a^2 + b^2 - 2 \cdot a \cdot b \cdot \cos(\theta)} \quad (11)$$

To calculate γ, the angle was split into the following angles, so it could be solved using triangles OAC and ABC:

$$\gamma = \angle OCA - \angle ACB \quad (12)$$

Therefore, letting $\angle$OCA be known as γ_1 and letting $\angle$ACB be known as γ_2.

To calculate γ_1, the cosine rule was used in the triangle OCA:

$$c^2 = e^2 + d^2 - 2 \cdot e \cdot d \cdot \cos(\gamma_1) \quad (13)$$

From equation 13, equation 14 is obtained for calculating γ_1:

$$\gamma_1 = \arccos\left(\frac{e^2 + d^2 - c^2}{2 \cdot e \cdot d}\right) \quad (14)$$

To calculate γ_2, the cosine rule is used in the triangle ABC:

$$b^2 = e^2 + a^2 - 2 \cdot e \cdot a \cdot \cos(\gamma_2) \quad (15)$$

From equation 15, equation 16 is obtained for calculating γ_1:

$$\gamma_1 = \arccos\left(\frac{e^2 + a^2 - b^2}{2 \cdot e \cdot a}\right) \quad (16)$$

C. Static Force Analysis Calculations

Static force analyses have been conducted using the kinematic analyses' results and by defining the load, which would be exerted onto the digits when in use. Static force analyses have been conducted rather than dynamic force analyses because the maximum stress experienced by the links on the digits is the maximum force which the digits can apply, which can only be experienced when the digits are static.

The static force analysis was conducted to represent the mechanisms when the linear actuators exerted maximum force. The analyses were performed by expressing the mechanisms as 2D diagrams—furthermore, expressing the moments and forces experienced by all the links. Static force analyses were not conducted on the asynchronous digits and the synchronous thumb since these parts are too complex.

D. Synchronous Digit Calculations

A static force analysis was performed on the index and ring fingers. The index and ring fingers contained the exact mechanism with the same dimensions; therefore, only one static force analysis was required. Fig. 5 shows the diagram of the synchronous digit with the external moments applied to the system:

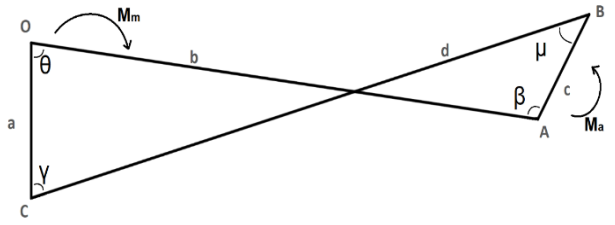

Figure 5. Diagram of static force analysis of synchronous index and ring fingers

The moment M_m is the moment created by the motor applying a force on the digit. The moment M_a is the moment that is created by the phalanges applying a force onto the object being gripped. The leverage arm for the moment is the length of the phalange connected to the proximal phalange. To evaluate the forces acting on each link, diagrams of each link have been drawn with the acting forces and moments, which can be seen in Fig. 6, Fig. 7, and Fig. 8:

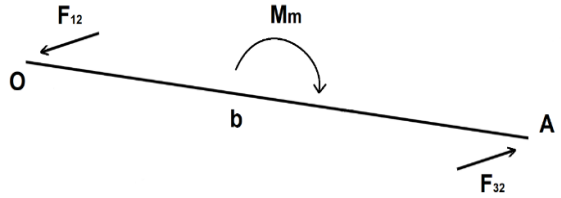

Figure 6. Diagram of the proximal phalange

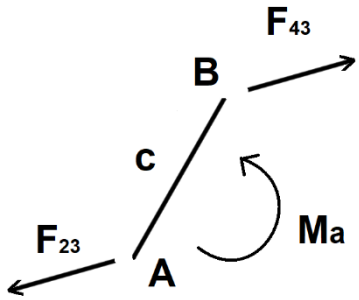

Figure 7. Diagram of PIP joint

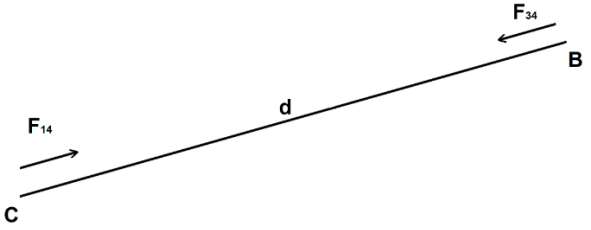

Figure 8. Diagram of connecting link

The moments and torques acting on the links are as follows:

F_{12} – Reaction force of link 1 acting on link 2
F_{32} - Reaction force of link 3 acting on link 2
F_{23} - Reaction force of link 2 acting on link 3
F_{43} - Reaction force of link 4 acting on link 3
F_{34} - Reaction force of link 3 acting on link 4
F_{14} - Reaction force of link 1 acting on link 4
M_m – Moment applied from the motor
M_a – Moment applied from the digit applying force on an object

As can be seen in Fig. 2, Fig. 3, and Fig. 4, the force is parallel with the link the force is being applied on. This correlation is because no moments are applied to the link, and Newton's first law states that every object shall remain motionless or in uniform motion unless an external force acts on it [26]. Since the link is motionless, the sum of all applied moments must be equal to zero (conservation of angular momentum). Therefore, the reaction forces being applied on the link must be parallel to the link.

As can be seen in Fig. 6, Fig. 7, and Fig. 8, the two reaction forces acting on the links are equal in magnitude but are opposite in direction. This is due to Newton's first law, which leads to the sum of all forces being equal to zero since the object is static [26]. Since all the links only have two forces acting on them, the two forces acting on the link must have an equal magnitude but an opposite direction (conservation of linear momentum).

The following equations can therefore be deduced:

$$|F_{32}| = |F_{43}| \tag{17}$$

$$|F_{43}| = |F_{34}| \tag{18}$$

The following equations are obtained from Newton's third law, which states that every action has an equal and opposing reacting action [26]. This causes all coupled reacting forces between links to have the same magnitude with opposite directions. The following equations can therefore be deduced:

$$|F_{12}| = |F_{32}| \tag{19}$$

$$|F_{23}| = |F_{43}| \tag{20}$$

$$|F_{34}| = |F_{14}| \tag{21}$$

Due to the conservation of angular momentum on a static body, the following equation was obtained from Fig. 4(a) for calculating M_a:

$$M_a = F_{43} \cdot c \cdot \cos(\mu) \tag{22}$$

Due to the conservation of angular momentum on a static body, the following equation was obtained from Fig. 3(b):

$$M_m = F_{12} \cdot b \cdot \cos(\gamma + \theta) \tag{23}$$

From Equation 23, the following equation is obtained for calculating F_{12}:

$$F_{12} = \frac{M_m}{b \cdot \cos(\gamma + \theta)} \tag{24}$$

E. Static Thumb Calculation

A static force analysis was performed on the static thumb. Fig. 9 shows the diagram of the static thumb with the external moments applied to the system:

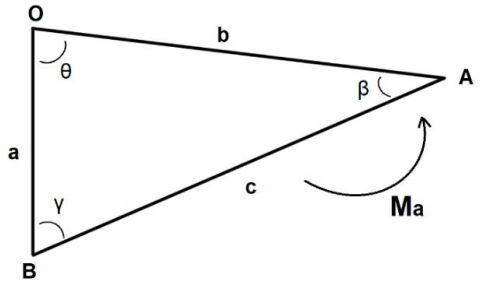

Figure 9. Diagram of static force analysis of static thumb

The force caused by the motor is not shown since the motor acts as one of the links. Therefore, the motor's force acts as a resultant force for that link. The moment M_a is the moment that is created by the phalanges applying a force onto the object being gripped. The leverage arm for the moment is the length of the phalanges. To evaluate the forces acting on each link, diagrams have been drawn with the acting forces and moments, which can be seen in Fig. 10 and Fig. 11.

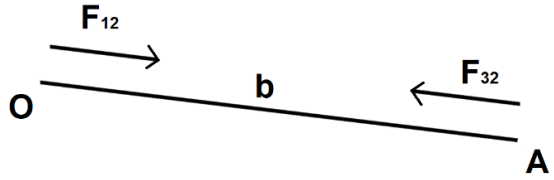

Figure 10. Diagram of motor

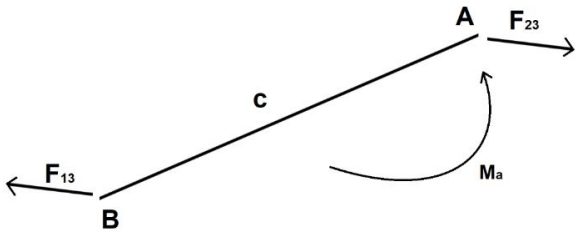

Figure 11. Diagram of bottom link

The moments and torques acting on the links are as follows:

F_{12} – Reaction force of link 1 acting on link 2
F_{32} - Reaction force of link 3 acting on link 2
F_{23} - Reaction force of link 2 acting on link 3
F_{13} - Reaction force of link 1 acting on link 3
M_a – Moment applied from the thumb applying force on an object

Similar to the synchronous digit, the rule applies to the system, where all coupled reacting forces between links have the same magnitude with opposite direction due to Newton's third law. Equation 25 is therefore deduced:

$$|F_{32}| = |F_{23}| \tag{25}$$

Due to the conservation of linear momentum, the magnitude of all acting forces on an object must be equal to zero. Since only two forces act on each link, the acting forces would be equal in magnitude but opposite in direction. The following equations are therefore deduced:

$$|F_{12}| = |F_{32}| \tag{26}$$

$$|F_{23}| = |F_{13}| \tag{27}$$

Since link b is the motor actuating the digit, the magnitude of the reaction force for a link be would be equal to the force of the motor (F_m). Equation 28 shows this relationship:

$$|F_{12}| = |F_m| \tag{28}$$

Due to the conservation of angular momentum, the sum of all moments acting on a body must equal to zero. The following equation is therefore obtained from Fig. 8 for calculating M_a:

$$M_a = F_{23} \cdot c \cdot \cos(\beta) \tag{29}$$

F. Kinematics and Static Force Analysis Programs and Results

Programs were developed in MATLAB 2014a to perform the kinematic analyses, static force analyses, and optimizations of the kinematic design of the Touch Hand 4. The previous calculations were used and incorporated in the program to perform the analyses automatically. It was decided to perform the analyses on MATLAB rather than manually for the following reasons:

- The kinematic analyses are capable of being simulated and animated. This helps to verify that the calculations are performed correctly.
- The program is capable of optimizing the design of the mechanism automatically
- Graphs are automatically generated and can be used to observe the results of analyses
- Calculating of the analyses is performed faster, which allowed for variations of the mechanisms to be tested and compared

The kinematics of the hand has been created to determine the angles. Thus, helping to place the digits, palm shape, and the angle ranges of the joints of the digits. The joint angles were selected to ensure that all the digits meet when all the digits are fully closed. A 3D stick figure of the Touch Hand 4 was generated using the dimensions obtained from the anthropomorphism survey (White, 1980). All joint angles and angles between the digits were incorporated into the program to be altered, thus manipulating the hand's kinematics.

The kinematic design for the prosthetic hand's index finger and ring finger is the same. Therefore, these two digits were analyzed together. Linear actuators actuate the rotation of these digits. A program was developed to analyse the kinematics as well as the force applied onto the digits from the linear actuator. The mechanism of the motor connected to the digit was animated and observed to aid the design process.

With the aid of the program, angles were chosen to define the orientation of the digits, as shown in Table I, which shows the angles obtained using the overall hand kinematics program.

TABLE I. CALCULATED ANGLES FOR DIMENSIONING OF TOUCH HAND 4

Angle between index and ring finger (°)	15
Angle between index finger and thumb (°)	110
Range of index and ring finger's MCP joint angle (°)	0-90
Range of index and ring finger's PIP joint angle (°)	0-60
Range of index and ring finger's DIP joint angle (°)	0-30
Range of thumb's MCP joint angle (°)	0-45
Range of thumb's PIP joint angle (°)	45-90
Thumb DIP joint angle (°)	45

The overall hand kinematics program determines the difference in the location in the X direction and Y direction of the tips of the digit. This program was done to ensure that when designing and modeling the digits, the tip of the digits would contact one another when performing a closed grip.

G. Index and Ring Finger

Two programs have been written for the kinematics of the index and ring fingers. The first program was written to simulate the kinematics of the link, which attaches the linear actuator to the digit. The second program was used to simulate the flexion of the synchronous digit.

The moment created by the linear actuator applying force onto the digit was required to be calculated and was therefore done so with the aid of a program, which simulated the link, which attaches the linear actuator to the digit. This program was created to ensure that the rotation of the MCP joint was performed to have a relationship with the linear actuator stroke length, which is as linear as possible. A linear relationship between the actuator stroke length and the MCP joint is desirable since a linear relationship would ensure that the digit rotates at a constant speed since the linear actuator moves at a constant speed. The program was also used to determine the required maximum stroke length of the mechanism, which was needed to configure the motor control system. The program was developed to be adjusted according to the rotation range of the MCP joint required. This program represents the kinematics for both static and synchronous digits. Fig. 12 shows an image from the animation of the simulated mechanic:

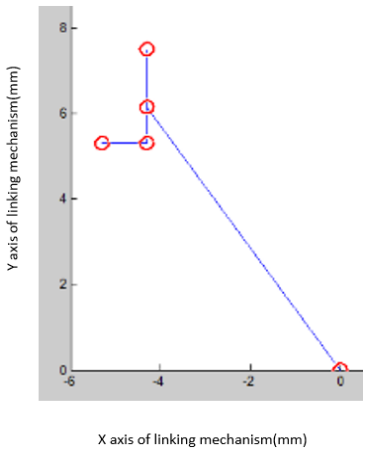

Figure 12. Motor link animation

Fig. 13 shows the relationship between the angle of the MCP joint and the stroke length of the linear actuator:

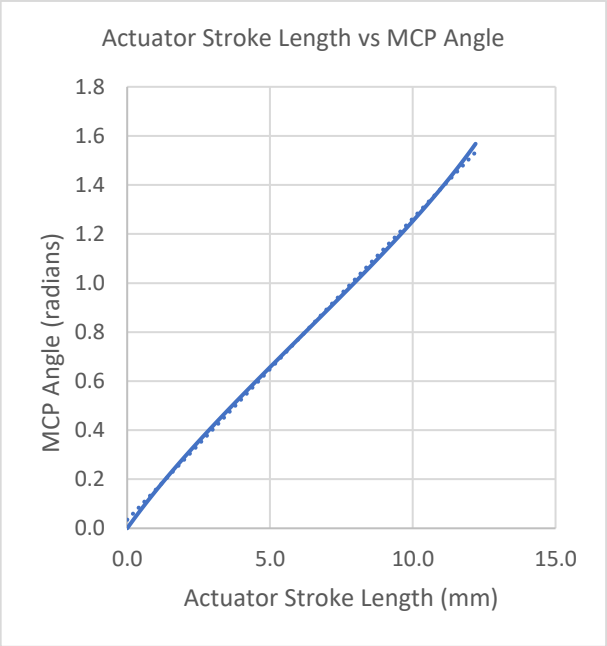

Figure 13. Graph of actuator stroke length vs. MCP joint angle of index and ring fingers

The graph in Fig. 13 can be seen to follow closely to its linear trend line. The relationship between the stroke length and the applied force of the index and ring finger can be seen in Fig. 14.

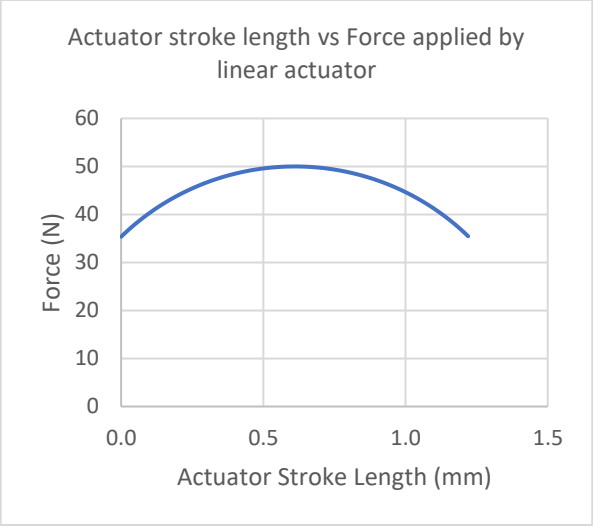

Figure 14. Graph of actuator stroke length vs. the applied force of index and ring fingers

Once the moment applied by the motor was determined, the program used to simulate the synchronous digit was created. This program was created for the following reasons:

- To calculate the dimensions for the linking mechanism according to the specified joint angle ranges and phalange lengths. The dimensions were optimized to ensure the digits could remain as thin as possible.

- To calculate the rotation of the joints relative to the linear actuator stroke length.
- To perform a static force analysis to calculate the axial and shear forces which would act on each link.
- To calculate the maximum force the digit can apply to an object.
- To animate the linking mechanism of the digits.

The linking mechanism was simulated to perform a simulation on a digit, which contained a moving DIP joint as well as a moving PIP joint. Since there is no movement in the static digit other than the MCP joint, no program was written to simulate it. Fig. 15 shows an image from the animation of the simulated mechanic.

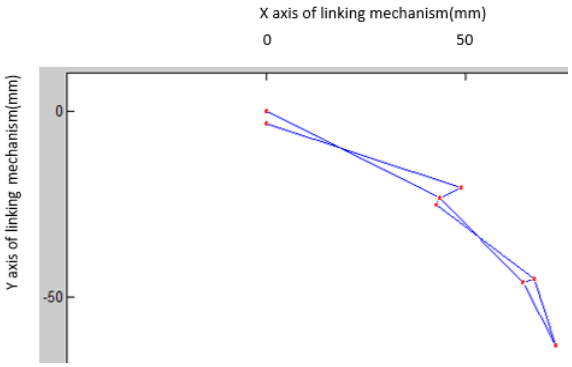

Figure 15. Synchronous index and ring finger animation

According to a review comparing the mechanical performance of commercial prosthetic devices, it was assumed that the relationship between the angle of the MCP joint and PIP joint should be linear. Data on the two angles were therefore obtained and compared [6]. Fig. 16 shows the relationship between the MCP and PIP joint angle.

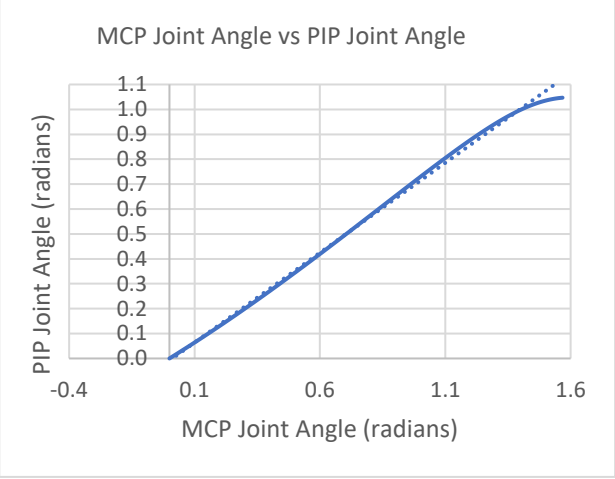

Figure 16. Graph of MCP joint angle vs. PIP joint angle of index and ring fingers

As shown in Fig. 16, the relationship between the two joint angles has a minor deviation from the linear trend line. The shape of the graph closely resembles the ones of the commercial prosthetic hands [6]. The relationship between the actuator stroke length and the DIP joint angle was also compared to determine whether it would be possible to incorporate a joint coupling mechanism to actuate the DIP joint. Fig. 17 shows the relationship between the actuator stroke length and the DIP joint angle:

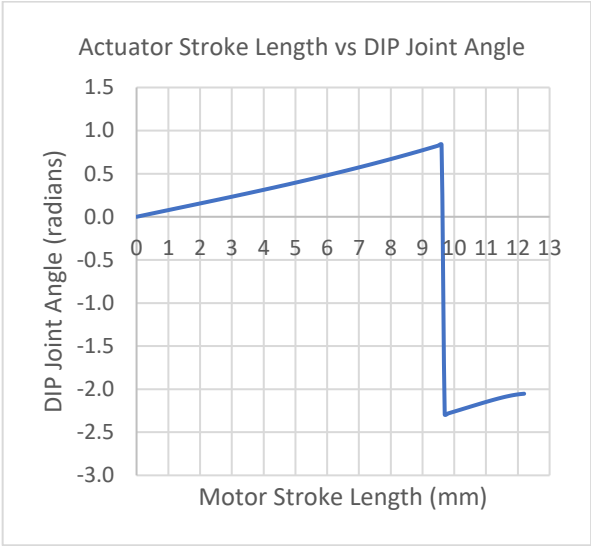

Figure 17. Graph of linear actuator stroke length vs. DIP joint angle of index and ring fingers

As shown in Fig. 17, the graph behaves irregularly when the actuator stroke length reaches 11.5 mm. This length is because the linking mechanism could not rotate the DIP joint angle to the specified angle range. Actuation of the DIP joint was abandoned in the design and was replaced with a 30 °bend in the link. Fig. 18 shows the forces which act on the links of the synchronous digits when applying maximum force on an object.

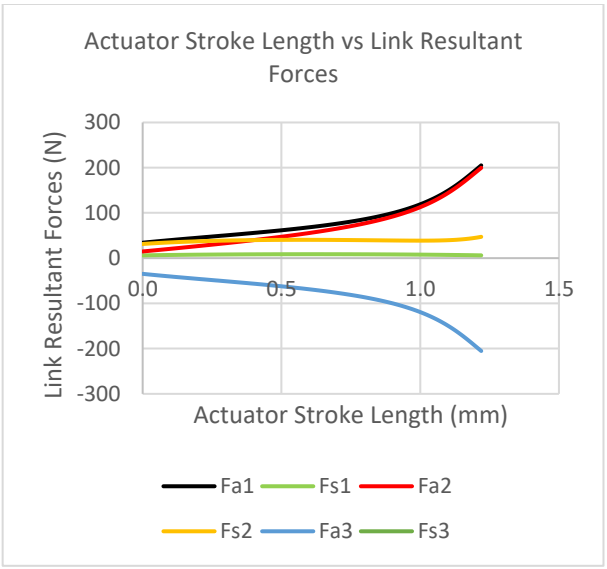

Figure 18. Graph of the synchronous index and ring finger link forces

The static force analysis calculated the resultant axial force and resultant shear force experienced on the three links in Fig. 5 when applying maximum force on an object. Fa1 and Fs1 are the forces experienced on link b, Fa2 and Fs2 are the forces experienced on link c, and Fa3 and Fs3 are the forces experienced on link d. The axial forces in

Fig. 18 (Fa1, Fa2, and Fa3) apply tensile stress on the link when it is positive and applying compressive stress on the link when it is negative. The shear forces in Fig. 18 (Fs1, Fs2, and Fs3) are applying shear stress in an anticlockwise direction on the link when it is positive and applying shear stress in a clockwise direction on the link when it is negative. The graph shows that the magnitude of the axial and shear forces are at the highest when the digits are fully closed.

H. Static and Synchronous Thumb

Three programs were written for the kinematics of the thumbs. The first program was written was to calculate the dimensions of the linking mechanism for the synchronous thumb, the second was used to simulate the flexion of the static thumb, and the third was used to simulate the flexion of the synchronous thumb.

The relationship between the links and the angle range for the thumb MCP joint was to be determined in the thumb linking mechanism. Thus, ensuring the digit kinematics are the same as those determined by the overall hand kinematics program. The program was developed to adjust the lengths of the links, while the CMC joint angle was at the end of its range to determine how the angle of the MCP joint changed. Fig. 19 shows an image from the animation of the simulated mechanic.

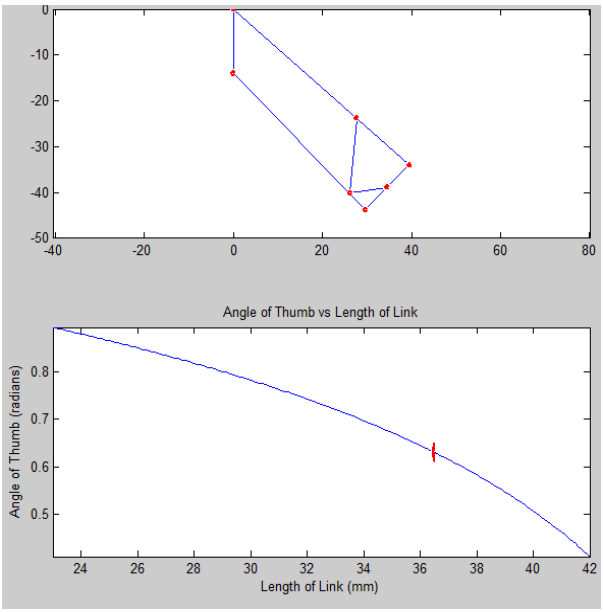

Figure 19. Synchronous thumb link animation

The link length was chosen from the graph in Fig. 19 according to the desired angle of the MCP joint. Once the dimensions were determined, the program to simulate the static thumb and the synchronous thumb were developed. These programs were created for the following reasons:

- To determine the required stroke length, which was required from the linear actuator, which was needed to configure the motor control system
- To calculate the rotation of the joints relative to the linear actuator stroke length.
- To perform a static force analysis to calculate the axial and shear forces which would act on each link.
- To animate the linking mechanism of the digits.

Fig. 20(a) shows an image from the animation of the simulated mechanic of the static thumb, and Fig. 20(b) shows an image from the animation of the simulated mechanic of the synchronous thumb.

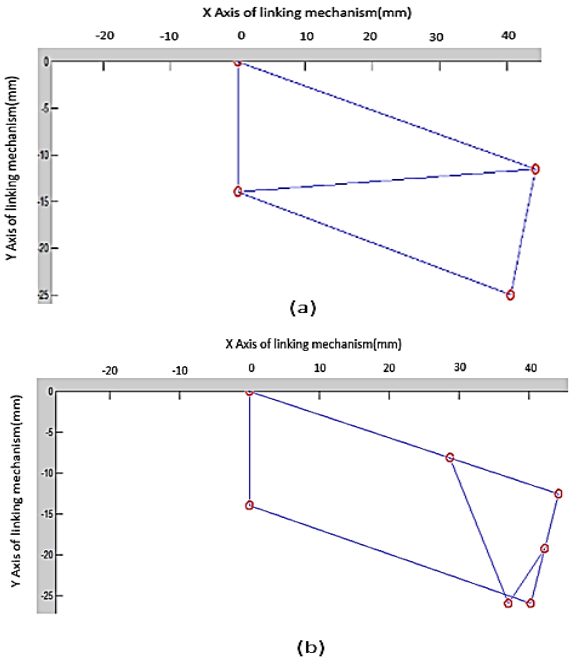

Figure 20. (a) Static thumb animation (b) Synchronous thumb animation

A linear relationship between the CMC joint and the linear actuator stroke length is desired to ensure that the rotation of the digit is performed at a constant speed. Fig. 21 shows the relationship between the angle of the CMC joint and the stroke length of the linear actuator of the static and synchronous thumb.

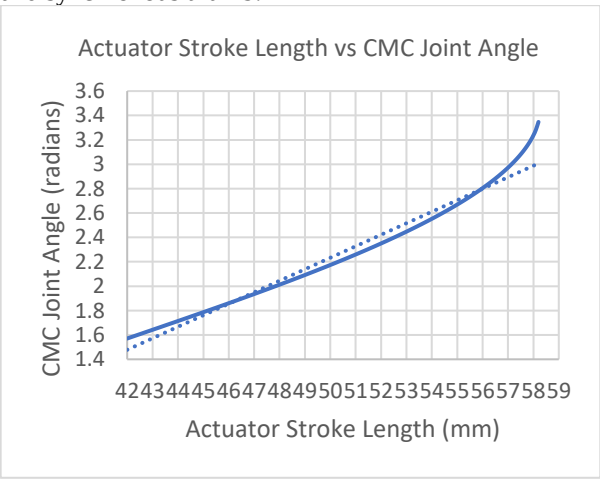

Figure 21. Graph of linear actuator stroke length vs. CMC joint angle of the thumb

As can be seen in Fig. 21, the relationship between the actuator stroke length and the CMC joint angle deviates from its linear trend line once the digit reaches the end of its range of rotation.

Similar to the synchronous index and ring fingers, it was interesting to determine the relationship between the two moving joints, which are the CMC and MCP joints in the

case of the thumb. Fig. 22 shows the relationship between the CMC and MCP joint angles of the synchronous thumb:

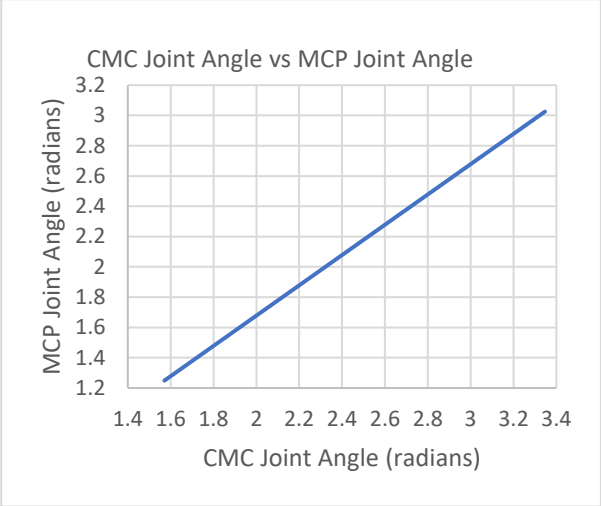

Figure 22. Graph of CMC joint angle vs. MCP joint angle of the synchronous thumb

As shown in Fig. 22, the relationship between the two joint angles appears to be linear.

Results from the static force analysis provided the resultant axial force and resultant shear force of all the links in Fig. 9 when applying maximum force on an object. Fig. 23 shows the forces that act on the static thumb's links when applying maximum force on an object.

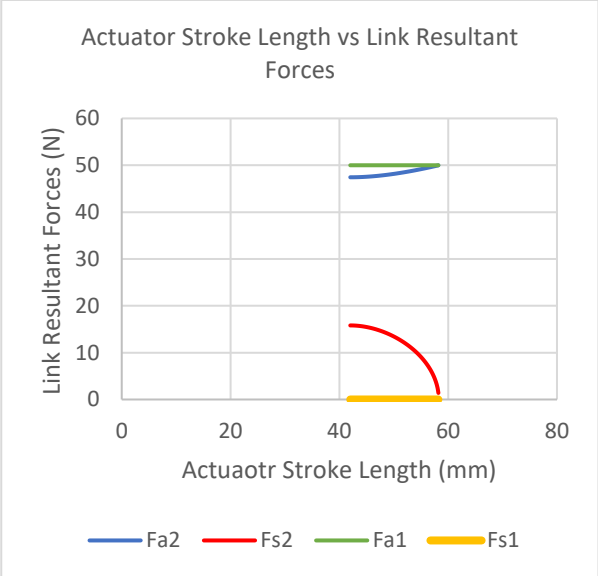

Figure 23. Graph of resultant link forces of static thumb

Similar to the static force analysis in the index and ring fingers, the axial forces in Fig. 23 are considered to apply tensile stress on the link when positive and compressive stress on the link when negative. The shear forces in Fig. 23 are considered to be applying shear stress in an anticlockwise direction on the link when it is positive and applying shear stress in a clockwise direction on the link when it is negative.

I. The Applied Force of Digits

The static force analyses were used to determine the applied force of each digit. The applied forces of the static index and ring fingers, the synchronous index and ring fingers, and the static thumb were compared to determine the digit that performs the best grip strength. Fig. 24 shows the graph which compares the maximum force which can be applied by these digits.

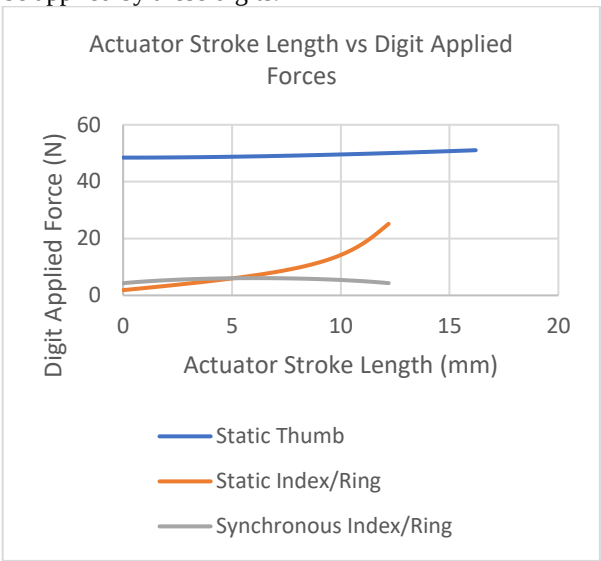

Figure 24. Graph of digit force applied of digits

Fig. 24 shows a significant variation in the performance of the digits. The synchronous index and ring fingers apply the lowest maximum force compared to all the digits but have a more consistent force relative to the linear actuator stroke length. The static index and ring fingers apply a higher force at the end of its range of rotation, but at the beginning, it is weaker than the synchronous digits. However, the beginning of the rotation range is of less concern since most objects would be gripped when the digits are at the end of the range of rotation. The static thumb shows to consistently applies a force throughout its range of rotation and shows to apply the strongest force in comparison to the other digits.

V. Tests and Results

Grip tests were performed on the prosthetic hand to determine the functionality of the mechanical system designed. The functionality of the mechanical device was tested by testing the device's adaptability to grip other objects and the overall grip strength.

The grip strength test was performed to compare the overall grip strength of the device with other commercial prosthetic devices and to evaluate the operation of the force control of the motor control system. The grip strength was performed by attaching a scale to the digits and observing the force the digits can apply.

The index and ring fingers' MCP joint were kept at 45 ° when tested, and the CMC joint of the thumb was kept at 22.5 ° when tested. These angles were chosen since they are in the middle of the joints' range of motion. The scale was attached to the index and ring finger, while the thumb

was kept static. The scale was then pulled until the digits were forcefully opened to determine the maximum grip of the hand. The maximum grip strength test was performed five times on the Touch Hand 4 using the static and synchronous digits. Synchronous digits showed an average of 17.2 N, while the static digits showed an average of 30.4 N.

Grip tests were performed on various objects, which were used to represent the aforementioned grip patterns. The objects used to perform the tests were chosen to represent the types of objects that each prehensile grip pattern would grip. Table II shows the digits used for the different objects gripped.

TABLE II. GRIP TESTING CRITERIA

Grip pattern	Object used in test	Digits used
Cylindrical grip	Spray bottle	Index, ring, thumb
Spherical grip	Apple	Index, ring, thumb
Hook grip	Backpack	Index, ring
Precision grip	Piece of pasta	Ring, thumb
Palmer grip	Piece of paper	Ring, thumb
Tripod grip	Pen	Ring, thumb
Flat grip	Book	Index, ring, thumb

The grips performed on the spray bottle, apple and backpack showed to grip the object securely. The thumb was used to make contact only on the side for the apple and spray can, as it was designed to be used—the angle as it allowed the digits to surround the apple from three sides. The angle between the digits showed little effect on gripping the spray can. The angle between the digits caused either the ring finger or the index finger to carry most of the load when carrying the backpack. This depended on the orientation of the prosthetic hand.

The grips performed on the piece of pasta, piece of paper, and pen only used the ring finger and thumb. The grips performed on the piece of pasta, and the piece of paper appeared to be secure as the objects were gripped using the padding added to the digits. The pen could not be securely gripped as it would swivel and rotate when trying to use the pen to write, yet improvements in the padding on the thumb would resolve this issue.

The grip performed on the book was successful; however, it failed to secure the object in the grip. The book was loosely gripped and led to the book slipping over the thumb. Again, the padding on top of the thumb would prevent slippage.

Tests were performed to determine the response time of the prosthetic hand to open and close the hand to determine the speed of the actuation mechanism. The close time average was 4.46 seconds, while the average open time was 2.93 seconds. The open response time and close response time measured were the time intervals between the instruction given to the amputee to open or close the hand and the actuation of the digits. The digit open time and digit close time were the time intervals between the beginning of the actuation of the digits and the end of the actuation of the digits. The time intervals were measured using a stopwatch.

To determine the competency of the prosthetic hand, it was compared with other prosthetic devices in terms of performance and specification of the devices, as shown in Table III.

TABLE III. PERFORMANCE AND SPECIFICATIONS COMPARISON

	Bebionic	i-Limb Ultra	Michelangelo	Touch Hand 4
Grip Strength (N)	36	136	70	30.4
Respon-siveness (s)	1.0	1.2	-	4.5

VI. CONCLUSION

Kinematic analysis played a vital role in the design of the mechanical system as it was used to determine the dimensions of the parts in the mechanical system. The grip tests performed on the objects showed that the proposed design of a prosthetic hand was fully capable of gripping objects of various sizes. However, the overall grip strength proved to be relatively weak in comparison to other prosthetic hands. Furthermore, the responsiveness test showed that the proposed design is flawed regarding moving its digits quickly due to the selected actuators.

Designs of digits, which use the same mechanisms used in the Touch Hand 4, therefore need not to perform the calculations for the kinematics and static force analysis from basic principles.

Table III shows that the grip strength of the designed prosthetic hand is within a similar range as the Bebionic prosthetic hand. However, the responsiveness is significantly slower than the other prosthetic devices analysed. The actuator used in the designed prosthetic hand is the Firgelli PQ12 linear actuator which limits the speed of the digits (Firgelli Technologies, 2018). The slow speed is due to the high gearing ratio of the motor, which directly affects the grip strength of the prosthetic hand.

The contributions that were in this paper allowed for the investigation of various designs for digits through the analysis of the design relative to prehensile grip patterns. The kinematics and statics analysis of the digits were performed with the kinematic analysis and static force analysis programs, showing the capability of the kinematics and static force analysis programs. The design of the mechanical system was proven to be functional by being capable of gripping objects of various sizes.

CONFLICT OF INTEREST

The authors declare no conflict of interest.

AUTHOR CONTRIBUTIONS

Kiran Setty designed the Touch Hand 4 and integrated the system. Theo van Niekerk supervised the work. Riaan Stopforth supervised and funded the work in preparation for the Cybathlon 2020 event. Karina Sewsunker compiled the paper and edited as needed. Anton du Plessis analyzed and edited the paper with the technical feedback required.

ACKNOWLEDGEMENT

The authors acknowledge the funding of this research by the South African Department of Science and Technology (DST) Robotics Strategy of South Africa (ROSSA) programme, Eskom TESP programme, the National Research Foundation (NRF), and Manufacturing, Engineering and Related services SETA (MerSETA). We also acknowledge the support and sponsorship of Rapid 3D, Horne Technologies, BunnyCorp, IDS Innovative Dental Solutions, and the Robotics Association of South Africa (RASA).

REFERENCES

[1] T. Kulkarni and R. Uddanwadiker, "Overview: Mechanism and Control of a Prosthetic Arm," *Molecular and Celluar Biology*, vol. 0, no. 0, pp. 1-49, 2015
[2] Ottobock, "The world's most advanced prosthetic hand - bebionic," 2018. [Online]. Available: http://bebionic.com/. [Accessed March 2018].
[3] D. P. M. O. T. Sheetz, *Technology's Helping Hand*, University of Pittsburgh, 2019.
[4] Touch Bionics, "Touch Bionics," Touch Bionics, 2018. [Online]. Available: http://touchbionics.com/. [Accessed March 2018].
[5] T. D. Telegraph, *Transplant Patient Receives Bionic Hand with Electronic Fingers*, 2013.
[6] J. T. Belter, J. L. Segil, A. M. Dollar, and R. F. Weir, "Mechanical design and performance specifications of anthropomorphic prosthetic hands: A review," *JRRD*, vol. 50, no. 5, pp. 599-618, 2013.
[7] Ottobock, "The world's most advanced prosthetic hand - bebionic," Ottobock, 2018. [Online]. Available: http://bebionic.com/. [Accessed March 2018].
[8] A. Mohammadi, J. Lavranos, H. Zhou, R. Mutlu, G. Alici, Y. Tan, P. Choong, and D. Oetomo, "A practical 3D-printed soft robotic prosthetic hand with multi-articulating capabilities," *PLOS ONE*, vol. 15, no. 5, 2020.
[9] M. Sullivan, B. Oh, and I. Taylor, "3d printed prosthetic hand," Washington University in St. Louis, St. Louis, 2017.
[10] A. R. A. R. S. G. Jones, "Prosthetic design directives: Low-cost hands within reach," in *Proc. International Conference on Rehabilitation Robotics*, London, UK, 2017.
[11] R. Fourie and R. Stopforth, "The mechanical design of a biologically inspired," *Touch Prosthetics*, 2016.
[12] All Answers Ltd., "The major function of human hand psychology essay," *UKEssays.com*, November 2017.
[13] E. F. Guilak, "Arches of the hand in reach to grasp," *Journal of Biomechanics*, vol. 41, p. 829, 2007.
[14] A. A. Fallahi and A. A. Jadidian, "The effect of hand dimensions, hand shape and some anthropometric characteristics on handgrip strength in male grip athletes and non-athletes," *Journal of Human Kinetics*, vol. 29, pp. 151-159, September 2011.
[15] R. M. White, "Comparative anthropometry of the hand," *Natick*, 1980.
[16] N. Jarque-Bou, V. Gracia-Ib áñez, J. L. Sancho-Bru, M. Vergara, A. P érez-Gonz ález, and F. J. Andr és, "Using kinematic reduction for studying grasping postures," *Applied Ergonomics*, vol. 56, pp. 53, 56, 2016.
[17] N. Van der Merwe, Interviewee. *Medical impact and design considerations for designing a pow-cost 3D printed prosthetic device.* [Interview]. 26 February 2018.
[18] C. L. Taylor and R. J. Schwarz, "The anatomy and mechanics of the human hand," *Artificial Limbs: A Review of Current Developments*, vol. 2, no. 2, pp. 24-28,32-34, 1955.
[19] R. F. A. R. Stopforth, "The mechanical design of a biologically inspired prosthetic hand, the touch hand 3," *Touch Prosthetics*, 2016
[20] A. Grundling, Interviewee. *Recommendations for design of a Low-Cost Prosthetic Arm Device.*. [Interview]. 14 June 2018
[21] R. Knight, Interviewee. *Design Requirements of a Myoelectric Prosthetic Hand.* [Interview]. 19 June 2018.
[22] C. Milne, Interviewee. *Advice on Design of a Low-Cost Myoelectric Prosthetic Hand.* [Interview]. June 2018.
[23] P. van der Walt, Interviewee. *Conceptual design of Touch Hand 4.* [Interview]. 18-22 February 2018.
[24] Firgelli Technologies Inc, "PQ12 - Datasheet," 2015. [Online]. Available: https://www.robotshop.com/media/files/PDF/pq12-datasheet.pdf. [Accessed March 2018].
[25] R. A. Adams and E. Christopher, *Calculus: A Complete Course*, 7 ed., Toronto, Ontario: Pearson Canada, 1940.
[26] M. Avadhanulu, *A Textbook of Engineering Physics*, New Delhi: S. Chand Publishing, 1992.

Riaan Stopforth, PhD, is involved with multi-disciplinary integration research. Research has been pursued in prosthetic devices, and in collaboration with Touch Prosthetics, the Touch Hand has participated in the 2020 Cybathlon

Theo van Niekerk, PhD, is involved with research involved with control systems, mechatronics, and vision system integration, with an interest in different research topics which has viable applications.

Kiran Setty completed his BSc Eng. (Mechanical) at UKZN and then completed MEng at Nelson Mandela University. He has an interest in different research areas and explored mechanical characteristics in prosthetic hands such as the Touch Hand.

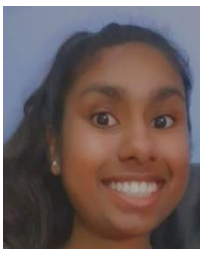

Karina Sewsunker studies mechanical engineering at the University of KwaZulu-Natal, with an interest in bio-mechatronic systems.

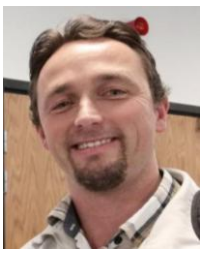

Anton du Plessis, PhD, has a great interest in complex additive manufacturing and identifying fatigue and defects in materials.